

Double-Walled ZrO₂ Nanotube Array: Preparation and Enhanced Photocatalytic Activity

Chaorui Xue,* Shengliang Hu, Qing Chang, Yanzhong Wang, and Jinlong Yang

This work demonstrates the formation of self-ordered double-walled ZrO₂ nanotube array via electrochemical anodization in glycerol-based electrolyte. Compared with its counterpart of single-walled ZrO₂ nanotube array, the tube wall of double-walled ZrO₂ nanotube split into outer and inner layers for the decomposition of glycerol during anodization process. Moreover, the double-walled structure showed its advantage of achieving improved utilization of light and higher specific surface area of nanotube array. Due to the unique double-walled structure, the double-walled ZrO₂ nanotube array exhibited better photocatalytic activity than the single-walled ZrO₂ nanotube array.

1. Introduction

Within the last decades, self-organized arrays of metal oxide nanotube (TiO₂, ZrO₂, and Fe₂O₃) have attracted a lot of research interests due to their outstanding physico-chemical properties compared to bulk metal oxide materials.^[1] Specially, these metal oxide nanotube arrays can be successfully obtained by anodization of corresponding metals such as Ti, Zr, and Fe.^[2–5] The particular advantages of anodic nanotube array are the high specific surface area and semi-conductive band gap. Metal oxide nanotube arrays can thus be used for photocatalysis. Notably, development of anodizing technique greatly promoted the preparation of anodic nanotube, and various advanced morphologies (e.g., bamboo, branched stacks, multilayers, and double wall) have been achieved.^[6–9] These unique morphologies can endow nanotube enhanced specific surface area and effective generation of electron–hole pairs. So higher photocatalytic properties can be achieved. For example, it has been reported by Ji^[10] that the anodic double-walled and bamboo type TiO₂ nanotube array exhibited higher specific surface area than single-walled nanotube array, and thus achieved higher performance on photocatalytic degradation of pollutants.

Among the unique morphologies of anodic nanotube, double-walled nanotube possesses tube wall consists of two diacritic

layers (inner layer and outer layer). In addition to aforementioned positive effects on the photocatalytic degradation of pollutants, Schmuki et al.^[11] reported that the double-walled structure could improve the thermal stability of TiO₂ nanotube array. Li et al.^[12] also found that the double-walled TiO₂ nanotube array demonstrated the potential of improving photoconversion efficiency in photoelectrochemical water splitting. Therefore, one could expect that the tube wall modulation can open a new avenue for enhancing applications of anodic metal oxide nanotube arrays. However, although ZrO₂ nanotube can also be obtained by anodization as TiO₂ nanotube,^[13,14] research progress in tailoring the morphology of anodic ZrO₂ nanotube is still behind that on anodic TiO₂ nanotube. To the best of our knowledge, the double-walled structure has not been reported for anodic ZrO₂ nanotube until now. This would limit the applications of ZrO₂ nanotube in many areas such as photocatalysis, sensors, and fuel cells.

In the present work, through anodization of Zr foils in glycerol-containing solution, double-walled ZrO₂ nanotube array was successfully obtained. Compared with single-walled ZrO₂ nanotube array, double-walled ZrO₂ nanotube array exhibited higher photocatalytic activity for its unique double-walled structure, which improved absorption of UV-Vis light and specific surface area of nanotube array. The formation mechanism of double-walled ZrO₂ nanotube array was also discussed based on the results of chemical composition measurement.

2. Experimental

A two electrodes system with working electrode of Zr foil and counter electrode of Pt foil was selected for the anodization experiment. Before anodization, Zr foils (0.3 mm thick, 99.8% purity) were firstly chemically polished in HF/HNO₃/H₂O (volume ratio, 1:4:2) solution, then washed with purified water, and dried under ambient atmosphere. The anodization process consisted of a voltage step of 0.1 V⁻¹ s⁻¹ from 0 V to end voltage of 80 V, followed by holding at this voltage for 1 h. Two different electrolytes were used, respectively. One electrolyte (solution 1) contained 57.9 g of glycerol, 0.3 g of NH₄F, and 1.8 g of H₂O. The other electrolyte (solution 2) contained 54.7 g of glycerol, 0.3 g of NH₄F, and 5 g of H₂O. After anodization, the obtained samples were washed with purified water for several times and dried under ambient atmosphere. Calcinations of

Dr. C. Xue, Prof. S. Hu, Dr. Q. Chang, Dr. Y. Wang, Prof. J. Yang
School of Materials Science and Engineering,
North University of China, Taiyuan 030051,
P. R. China
E-mail: crxue87@126.com

Prof. J. Yang
School of Materials Science and Engineering,
Tsinghua University, Beijing 100084, P. R. China

DOI: 10.1002/pssa.201700239

samples were conducted at 500 °C for 2 h with heating and cooling rate of 5 °C min⁻¹ under air condition.

Morphologies and chemical compositions of samples were characterized using scanning electron microscope (SEM, JSM-7001F), transmission electron microscope (TEM, JEM-2100F) and X-ray photoelectron spectrometer (XPS, AXIS ULTRA DLD). X-ray diffraction (XRD) patterns were obtained on an X'pert Philips PMD diffractometer at a scan rate of 0.03° s⁻¹. BET specific surface area measurements were carried out on a basis of N₂ adsorption by using a JW-BK300 surface area and porosity analyzer. UV-Vis diffuse reflectance spectra of samples were recorded using a UV-Vis spectrophotometer (UV-2550) equipped with an integrating sphere assembly and using BaSO₄ as reference. For photocatalytic experiments, samples of 1 cm² reaction area were put into a quartz cell containing 4 mL of methylene blue (MB) solution with concentration of 1 ppm. A 500 W Xe lamp was employed as light source. The light was passed through a glass filter of QD254 for achieving UV light irradiation. The absorbance of solution was measured every 30 min for 3 h with a UV-Vis spectrometer (UV-2550). The absorption maximum of methylene blue showed a peak at 664 nm (see Figure S2, Supporting Information). Analysis of hydroxyl radicals (•OH) was conducted by the photoluminescence technique using terephthalic acid (TA) as probe molecule. The concentration of TA was 4 × 10⁻⁴ mol L⁻¹ in 4 × 10⁻³ mol L⁻¹ NaOH solution. The photoluminescence spectra of reaction solution at 425 nm were measured every 10 min with 315 nm excitation. Other procedures were similar to the measurement of photocatalytic properties.

3. Results and Discussion

The content of solution has a profound impact on nanotube morphology. Using solution 1, a double-walled ZrO₂ nanotube array (DZNA) was obtained. Initially, highly ordered nanotubular structure can be clearly observed from the surface and lateral images of **Figure 1a** and **b**. Secondly, a double-walled structure was identified in TEM images of **Figure 1c** and **d**.

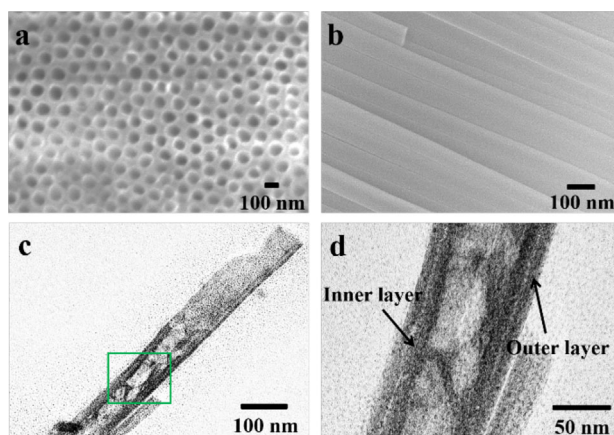


Figure 1. (a and b) SEM and (c and d) TEM images of the as obtained sample of DZNA. Panel (d) is the enlarged image of square area in panel (c).

Clearly, the tube wall of nanotube exhibits double-layered architecture, which contains inner and outer layers inside. The inner layer is enclosed in the outer layer. Both layers show similar thickness of about 16 nm (**Figure 1d**). Differently, using solution 2, single-walled ZrO₂ nanotube array (SZNA) was achieved. Although surface and lateral morphologies of nanotube array in **Figure 2a** and **b** showed similar tube diameter of around 120 nm as nanotube array shown in **Figure 1a** and **b**, there is only one dense single layer of tube wall (**Figure 2c** and **d**). Outer and inner layers, which are distinct in **Figure 1c** and **d**, cannot be observed. Therefore, double-walled ZrO₂ nanotube array was prepared in glycerol solution with low water content, while single-walled ZrO₂ nanotube array was obtained using electrolyte with high water content. In fact, the formation of anodic ZrO₂ nanotube array is strongly related to various experimental parameters such as anodization voltage, time, and solution content.^[15] Here, anodization voltage, time, and concentration of NH₄F are the same for samples of SZNA and DZNA, the only difference in anodization procedures is the ratio of glycerol content to water content in the solution. So it can be speculated that the double-walled structure could be formed due to the participation of glycerol and/or water through chemical reactions during anodization process. Detailed formation mechanism of the double-walled structure will be discussed below.

XPS was used to investigate the differences in chemical compositions of the single and double-walled ZrO₂ nanotube arrays. **Figure S1a**, Supporting Information shows the comparable wide scanning XPS spectra of samples of SZNA and DZNA. Both the single and double-walled ZrO₂ nanotube arrays showed clear constituents of elements Zr, C, O, and F. Apparently, carbon peak intensity for sample of DZNA is higher than that for sample of SZNA. This indicates that double-walled ZrO₂ nanotube array may suffer higher carbon contamination than single-walled ZrO₂ nanotube array during anodization process. Since glycerol is the only carbon source, in combination with investigations on double-walled TiO₂ nanotube array, it can be proposed that double-walled ZrO₂ nanotube array

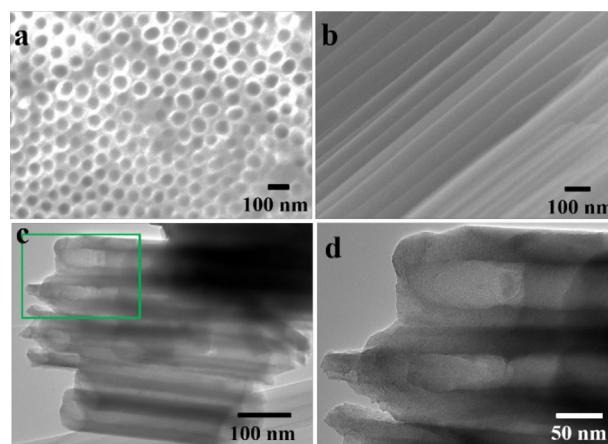


Figure 2. (a and b) SEM and (c and d) TEM images of the as obtained sample of SZNA. Panel (d) is the enlarged image of square area in panel (c).

should be formed for the decomposition of glycerol in the electrolyte.^[16] If water content is low, a thin oxide barrier layer will be primarily formed and produce high electrical field inside.^[17] Under high electrical field, tunneling in the schottky barrier layer may occur and generate holes.^[18] The holes are strong oxidative agents and can cause glycerol decomposition.^[19] At the electrolyte–ZrO₂ interface, the decomposition products of glycerol (e.g., glyceric acid, glycolaldehyde) will react with ejected Zr⁴⁺ and form the inner layer of tube wall.^[20] Meanwhile, the primarily formed thin barrier layer will form the outer layer, double-walled structure is thus finally developed. Whereas, if water content become higher, the barrier layer will grow thicker, decomposition of glycerol can hardly occur for the reduced electrical field. Thus single-walled structure is formed. The decomposition of glycerol was further confirmed by the narrow scanning XPS spectra of C1s. After deconvolution of C1s peak, though the distribution of signals is similar for both samples of SZNA and DZNA, the intensity of each signal differs obviously. As shown in **Figure 3a** and **b**, the C1s peak consists of three contributions (288.7, 286.6, and 284.8 eV) for both samples of SZNA and DZNA. The binding energy of 284.8 eV is due to adventitious carbon, while the binding energy of 286.6 and 288.7 eV should be due to the formation of carbonates for the decomposition of glycerol.^[21] Clearly, the peak intensities at 286.6 and 288.7 eV are higher for sample of DZNA than that for sample of SZNA. The inner layer of DZNA, which is formed due to the glycerol decomposition, should be responsible for the higher content of carbonates. Furthermore, elemental composition measurement has also been performed perpendicular to a double-walled nanotube (**Figure 3c**), the results are shown in **Figure 3d**. Obviously, the content of oxygen and carbon in the inner layer region is higher than that in the outer layer region. This further confirms the formation of carbonates in the inner layer which shows the accumulation of carbon and oxygen inside.

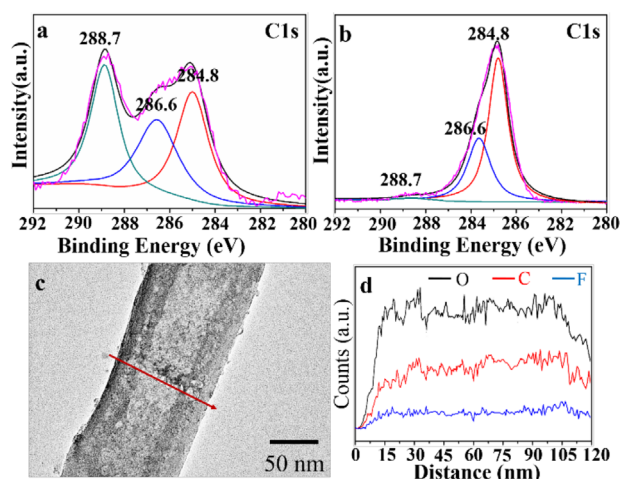


Figure 3. (a and b) Narrow scanning XPS spectra of C1s of as obtained samples of SZNA and DZNA. (a) DZNA, (b) SZNA. (c and d) TEM image and EDX spectra of O, C, and F for double-walled ZrO₂ nanotube. Panel (d) was obtained by taking EDX measurement following red line shown in panel (c).

Figure 4a and **b** show the XRD and UV-Vis absorption profiles for samples of DZNA and SZNA after calcination at 500 °C for 2 h. Clearly, both the single and double-walled ZrO₂ nanotube arrays transferred to a mixture of monoclinic and tetragonal phases after annealing. As shown in **Figure 4a**, both samples exhibited similar peaks of monoclinic and tetragonal phases. Moreover, in **Figure 4b**, both samples demonstrated primary absorption of ultraviolet light below 350 nm. This is caused by the intrinsic band gap of 5.7–7.2 eV for ZrO₂.^[22] Interestingly, it should be noted that enhanced absorption in the ultraviolet and visible light regions appeared for double-walled ZrO₂ nanotube array. This could be attributed to the double-walled structure. As shown in **Figure 4c**, after calcination, not only nanotube but also double-walled structure can be clearly identified for sample of DZNA. Differently, the sample of SZNA still exhibited a dense, single-walled structure (**Figure 4d**). Under UV-Vis light irradiation, the porosity of tube wall for the double-walled structure can significantly improve the scattering of light inside nanotube.^[23] So double-walled ZrO₂ nanotube array exhibited more promising UV-Vis absorption than single-walled ZrO₂ nanotube array.

The annealed samples of DZNA and SZNA also demonstrated different specific surface area. As shown in nitrogen adsorption–desorption isotherms of **Figure 4e**, the BET surface area of sample of DZNA is 49.250 m² g⁻¹, which is significantly higher than that of sample of SZNA (31.595 m² g⁻¹). The main reason for the enhanced specific surface area of sample of DZNA should be the double-walled structure. Tube wall of sample of DZNA splits into two layers, secondary pores are formed inside, enlarged specific surface area can thus be attained. Due to the

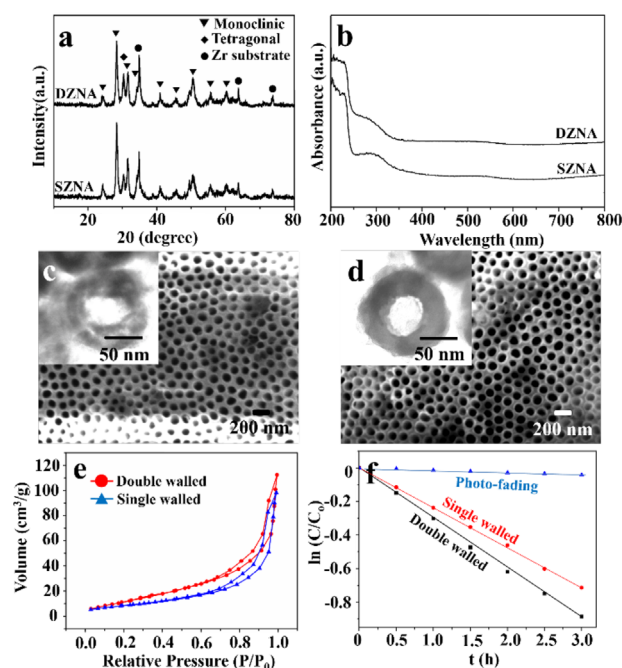
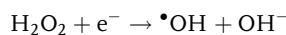
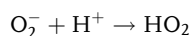
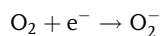
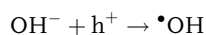
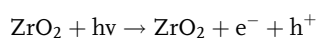


Figure 4. (a) XRD patterns, (b) UV-Vis absorption profiles, (c and d) SEM and inset TEM images, (e) BET adsorption–desorption isotherms, and (f) Pseudo-first-order kinetic rate plots of the photocatalytic degradation of MB solution for samples of DZNA and SZNA after annealing at 500 °C for 2 h.

enhanced specific surface area and UV-Vis light absorption property for the double-walled structure, the photocatalytic activity of double-walled ZrO₂ nanotube array is higher than that of single-walled ZrO₂ nanotube array. The photocatalytic test was conducted by studying the decomposition of methylene blue (MB), and the data in Figure 4f were plotted on a logarithmic scale for the time-dependent MB concentration shown in Figure S2, Supporting Information. In Figure 4f, a linear characteristic is observed for each experiment which indicates that the decomposition kinetics follows the first order law of $\ln(C/C_0) = kt$, where k is the pseudo-first-order rate constant and t is the time.^[24] It is not surprising that the degradation of MB was greatly improved by ZrO₂ nanotube. Under UV light irradiation, electron-hole pairs will be formed. The holes can react with OH⁻ ions, electrons may react with O₂.^[25] The hydroxyl radicals ([•]OH), which are strong oxidizing agents, will be created and decompose methylene blue in aqueous solution.^[26] The complete process can be understood with following chemical reactions:^[27]



Notably, it can also be observed that the degradation rate constant of MB is higher for sample of DZNA than that for sample of SZNA ($k_{\text{DZNA}} = -0.30 \text{ h}^{-1} > k_{\text{SZNA}} = -0.22 \text{ h}^{-1}$). This indicates the photocatalytic activity of double-walled ZrO₂ nanotube array is higher than that of single-walled ZrO₂ nanotube array. As discussed above, the double-walled structure not only improved the utilization efficiency of incident light, but also increased the specific surface area of nanotube. Upon ultraviolet light irradiation, more electron-hole pairs will be generated for the double-walled ZrO₂ nanotube array compared to the single-walled ZrO₂ nanotube array. The increased specific surface area of double walled ZrO₂ nanotube array can provide more surface sites for the adsorption of MB molecules.^[28] Therefore, double-walled ZrO₂ nanotube array exhibited better photocatalytic activity than single-walled ZrO₂ nanotube array for the unique double-walled structure.

Figure 5 shows the comparison of photoluminescence intensities of TA solution for samples of SZNA and DZNA. It can be easily observed that the photoluminescence intensity

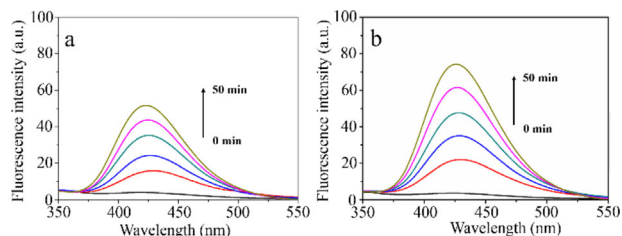


Figure 5. Fluorescence spectral changes of TA solution observed during illumination of samples of (a) SZNA and (b) DZNA.

increases faster for sample of DZNA than sample of SZNA. Herein, since the concentration of terephthalic acid is very low, they should be mainly oxidized by [•]OH.^[29] The reaction between terephthalic acid and [•]OH will produce 2-hydroxyterephthalic acid with significant fluorescence.^[30] So the fluorescence is from the chemical reactions between terephthalic acid and [•]OH photo-generated at the ZrO₂/water interface.^[31] Under ultraviolet light illumination, the double-walled structure, which showed porosity of tube wall, could cause light scattering inside, and improve the light utilization efficiency.^[32] More photons will be absorbed by double-walled ZrO₂ nanotube array, a larger number of electron-hole pairs will thus be formed and generate [•]OH according to above mentioned chemical reactions. Therefore, the formation rate of [•]OH on double-walled ZrO₂ nanotube array is higher than that on single-walled ZrO₂ nanotube array. Moreover, the specific surface area of double-walled ZrO₂ nanotube array is also higher than that of single-walled ZrO₂ nanotube array. The access of terephthalic acid to [•]OH can be enhanced by the double-walled structure. Considering above discussion, the double-walled structure is benefit for generating more [•]OH for ZrO₂ nanotube array during photocatalytic process. The [•]OH are strong oxidizing agents for methylene blue decomposition, so higher photocatalytic property of ZrO₂ nanotube array can be achieved for the double-walled structure.

4. Conclusion

In summary, double-walled ZrO₂ nanotube array was prepared by anodization in glycerol solution with low water content. The tube wall of nanotube contains outer and inner layers inside. The double-walled structure should be formed for the decomposition of glycerol, which causes the incorporation of carbon compared to single walled ZrO₂ nanotube. Due to the double-walled structure, after calcination, the double-walled ZrO₂ nanotube array exhibited enhanced UV-Vis light absorption property and specific surface area. The photocatalytic experiment also showed that the double walled ZrO₂ nanotube array holds better photocatalytic activity than single-walled ZrO₂ nanotube array for the unique layered architecture of tube wall.

Supporting Information

Supporting Information is available from the Wiley Online Library or from the author.

Acknowledgements

This work was supported by the National Natural Science Foundation of China (grant no. 51602292) and the starting fund for scientific research of North University of China (grant no. 130082).

Conflict of Interest

The authors declare no conflict of interest.

Keywords

double walled, oxidation, photocatalysis, porous materials, ZrO₂ nanotubes

Received: April 19, 2017
Revised: August 23, 2017
Published online:

-
- [1] S. Berger, F. Jakubka, P. Schmuki, *Electrochem. Commun.* **2008**, *10*, 1916.
- [2] H. Tsuchiya, J. M. Macak, A. Ghicov, L. Taveira, P. Schmuki, *Corros. Sci.* **2005**, *47*, 3324.
- [3] H. Tsuchiya, J. M. Macak, L. Taveira, P. Schmuki, *Chem. Phys. Lett.* **2005**, *410*, 188.
- [4] J. M. Macak, H. Tsuchiya, A. Ghicov, K. Yasuda, R. Hahn, S. Bauer, P. Schmuki, *Curr. Opin. Solid State Mater. Sci.* **2007**, *11*, 3.
- [5] K. Lee, A. Mazare, P. Schmuki, *Chem. Rev.* **2014**, *114*, 9385.
- [6] S. T. Nishanthi, B. Sundarakannan, E. Subramanian, D. Pathinettam Padiyan, *Renew. Energy* **2015**, *77*, 300.
- [7] V. C. Anitha, A. N. Banerjee, S. W. Joo, B. K. Min, *Mater. Sci. Eng. B* **2015**, *195*, 1.
- [8] D. S. Guan, Y. Wang, *Nanoscale* **2012**, *4*, 2968.
- [9] C. Xue, T. Yonezawa, M. T. Nguyen, X. Lu, *Langmuir* **2015**, *31*, 1575.
- [10] Y. Ji, *RSC Adv.* **2014**, *4*, 40474.
- [11] S. P. Albu, A. Ghicov, A. Aldabergenova, P. Drechsel, D. LeClere, G. E. Thompson, J. M. Macak, P. Schmuki, *Adv. Mater.* **2008**, *20*, 4135.
- [12] H. Li, J. Xing, Z. Xia, J. Chen, *RSC Adv.* **2014**, *4*, 23214.
- [13] Y. Shin, S. Lee, *Nanotechnology* **2009**, *20*, 105301.
- [14] X. Wang, J. Zhao, X. Hou, Q. He, C. Tang, *J. Nanomater.* **2012**, *2012*, 343.
- [15] K. Lee, A. Mazare, P. Schmuki, *Chem. Rev.* **2014**, *114*, 9385.
- [16] N. Liu, H. Mirabolghasemi, K. Lee, S. P. Albu, A. Tighineanu, M. Altomare, P. Schmuki, *Faraday Discuss.* **2013**, *164*, 107.
- [17] C. Xue, T. Narushima, Y. Ishida, T. Tokunaga, T. Yonezawa, *ACS Appl. Mater. Interfaces* **2014**, *6*, 19924.
- [18] Y. Y. Song, P. Roy, I. Paramasivam, P. Schmuki, *Angew. Chem.* **2010**, *122*, 361.
- [19] K. Okada, Electrochemical Oxidation of Glycerol in a Proton-Exchange-Membrane Reactor. Ph.D. Thesis, The University of Michigan, Ann Arbor, MI, USA, **2013**.
- [20] F. Roboni, N. T. Nguyen, S. So, P. Schmuki, *Nanoscale Horiz.* **2016**, *1*, 445.
- [21] E. Papirer, R. Lacroix, J. B. Donnet, G. Nansé, P. Fioux, *Carbon* **1995**, *33*, 63.
- [22] D. Fang, Z. Luo, S. Liu, T. Zeng, L. Liu, J. Xu, Z. Bai, W. Xu, *Opt. Mater.* **2013**, *35*, 1461.
- [23] Y. Liu, K. Mu, G. Yang, H. Peng, F. Shen, L. Wang, S. Deng, X. Zhang, Y. Zhang, *New J. Chem.* **2015**, *39*, 3923.
- [24] J. Zhang, Y. Wang, C. Yu, X. Shu, L. Jiang, J. Cui, Z. Chen, T. Xie, Y. Wu, *New J. Chem.* **2014**, *38*, 4975.
- [25] A. Houas, H. Lachheb, M. Ksibi, E. Elaloui, C. Guillard, J. M. Herrmann, *Appl. Catal. B* **2001**, *31*, 145.
- [26] H. Gnaser, M. R. Savina, W. F. Calaway, C. E. Tripa, I. V. Veryovkin, M. J. Pellin, *Int. J. Mass Spectrom.* **2005**, *245*, 61.
- [27] S. Kumar, A. K. Ojha, *J. Alloy Compd.* **2015**, *644*, 654.
- [28] B. Lu, X. Li, T. Wang, E. Xie, Z. Xu, *J. Mater. Chem. A* **2013**, *1*, 3900.
- [29] K. Ishibashi, A. Fujishima, T. Watanabe, K. Hashimoto, *Electrochem. Commun.* **2000**, *2*, 207.
- [30] K. Okamoto, Y. Yamamoto, H. Tanaka, A. Itaya, *Bull. Chem. Soc. Jpn.* **1985**, *58*, 2015.
- [31] J. Yu, G. Dai, B. Cheng, *J. Phys. Chem. C* **2010**, *114*, 19378.
- [32] Y. T. Ma, Y. A. Lin, X. R. Xiao, X. P. Li, X. W. Zhou, *Chin. Sci. Bull.* **2005**, *50*, 1985.